Transmembrane Helical Domain of the Cannabinoid CB_1 Receptor

Joong-Youn Shim*
J. L. Chambers Biomedical/Biotechnology Research Institute, North Carolina Central University, Durham, North Carolina

ABSTRACT Brain cannabinoid (CB_1) receptors are G-protein coupled receptors and belong to the rhodopsin-like subfamily. A homology model of the inactive state of the CB_1 receptor was constructed using the x-ray structure of β_2-adrenergic receptor (β_2AR) as the template. We used 105 ns duration molecular-dynamics simulations of the CB_1 receptor embedded in a 1-palmitoyl-2-oleoyl-*sn*-glycero-3-phosphocholine (POPC) bilayer to gain some insight into the structure and function of the CB_1 receptor. As judged from the root mean-square deviations combined with the detailed structural analyses, the helical bundle of the CB_1 receptor appears to be fully converged in 50 ns of the simulation. The results reveal that the helical bundle structure of the CB_1 receptor maintains a topology quite similar to the x-ray structures of G-protein coupled receptors overall. It is also revealed that the CB_1 receptor is stabilized by the formation of extensive, water-mediated H-bond networks, aromatic stacking interactions, and receptor-lipid interactions within the helical core region. It is likely that these interactions, which are often specific to functional motifs, including the S(N)LAxAD, D(E)RY, CWxP, and NPxxY motifs, are the molecular constraints imposed on the inactive state of the CB_1 receptor. It appears that disruption of these specific interactions is necessary to release the molecular constraints to achieve a conformational change of the receptor suitable for G-protein activation.

INTRODUCTION

According to the well-known two-stage model of integral membrane protein (IMP) folding (1), individual helical segments, upon insertion into the membrane, form stable α-helices in the first stage and then associate into a helical bundle in the second stage. This model was extended to include additional stages for loop association, ligand binding, or domain insertion (2). In support of this model, it was demonstrated that the entire structures of bacteriorhodopsin and rhodopsin are reconstructed from the individual helical segments (3,4). Thus, it appears that helical bundles are largely stabilized by interhelical interactions (1,5). However, failure in refolding into the helical bundle in some other cases (6,7) suggests that other interactions with neighboring structural elements, such as the interconnecting loops, surrounding lipids, and solvents, are also important for the folding of multispanning IMPs (8–10).

G-protein coupled receptors (GPCRs) are IMPs that are composed of seven transmembrane (TM) helices (H1–H7) interconnected by three intracellular loops (I1–I3) and three extracellular loops (E1–E3) (11). GPCRs are known to be among the most important drug targets (12). Despite of the overall low sequence homology (13), highly conserved amino acid residues in the TM helical domains (14) are indicative of common structure or functions in GPCRs (15,16). Recent publications of the x-ray crystal structures of opsin (17), rhodopsin (18), β_1AR (19), and β_2AR (20) have helped greatly to elucidate the GPCRs' function, showing that these x-ray structures share a quite similar topology overall but also distinct local structural differences.

Brain cannabinoid (CB_1) receptors with a total of 472 amino acid residues (21) have seven TM helices, like other GPCRs (22), and belong to the rhodopsin-like subfamily (11), which suggests that they have a molecular mechanism for G-protein activation similar to that in rhodopsin or β_2AR (11). The CB_1 receptor is known to mediate numerous physiological processes in response to marijuana and other psychoactive compounds (23). In the CB_1 receptor, many functional motifs are conserved as in rhodopsin and β_2AR (Table 1).

In the study presented here, a long molecular-dynamics (MD) simulation was used to explore the helical bundle structure of the inactive form of the CB_1 receptor to determine the molecular determinants of inter- and intrahelical stabilization. The results revealed that interhelical interactions specific to many of the functional motifs exist within the bilayer. It appears that disruption of these specific interactions would be necessary to release the molecular constraints imposed on the inactive state of the receptor to achieve a conformational change of the receptor suitable for G-protein activation. Thus, this study of the inactive form of the CB_1 receptor helps to lay the foundation for future studies on the molecular mechanism of G-protein activation in comparison with the active form of the CB_1 receptor. In this work, a numbering system similar to the Ballesteros-Weinstein system (15) is used for all of the amino acids.

MATERIALS AND METHODS

Homology model building

The sequence alignment program T-Coffee (http://www.tcoffee.org/) (24) was used to align the CB_1 receptor sequence to 19 subgroups (25) of rhodopsin-like GPCRs according to the highly conserved residues within

Submitted October 31, 2008, and accepted for publication December 30, 2008.

*Correspondence: jyshim@nccu.edu

Editor: Benoit Roux.

0006-3495/09/04/3251/12 $2.00

doi: 10.1016/j.bpj.2008.12.3934

TABLE 1 Helical boundaries of the x-ray structure of β_2AR (20) and the aligned, corresponding sequences of the CB_1 receptor used to construct the homology model for this study

Helix	Receptor	Start residue	Sequence	End residue
H1	β_2AR	30	EVWVVGMGIVMSLIVLAIVF**GN**VL**V**ITAIAK	60
	CB_1	113	PSQQLAIAVLSLTLGTFTVLE**N**LL**V**LCVILH	143
H2	β_2AR	67	VTNYFIT**SLA**C**AD**LVMGLAVVPFGAAHILM	96
	CB_1	151	PSYHFIG**SLA**V**AD**LLGSVIFVYSFIDFHVF	180
H3	β_2AR	103	NFWCEFWTSIDVLCVTA**S**IET**L**CVI**A**V**DRY**FAIT	136
	CB_1	186	RNVFLFKLGGVTASFTA**S**VGS**L**FLT**A**I**DRY**ISIH	219
H4	β_2AR	147	KNKARVIILMV**W**IV**S**GLTSFL**P**IQM	171
	CB_1	230	RPKAVVAFCLM**W**TI**A**IVIAVL**P**LLG	254
H5	β_2AR	197	QAYAIASSIVS**F**YV**P**LVI**M**VFV**Y**SR**V**FQEAKRQ	229
	CB_1	272	DETYLMFWIGVTSVLLLF**I**VYA**Y**MY**I**LWKAHSH	304
H6	β_2AR	266	LKEH**K**ALKTLGIIMGT**F**TL**CW**L**P**FFIVNIVHVI	298
	CB_1	336	RMDI**R**LAKTLVLILVVLII**CW**G**P**LLAIMVYDVF	368
H7	β_2AR	305	KEVYILLNWIGYV**NS**GF**NP**LI**Y**C	327
	CB_1	376	KTVFAFCSMLCLL**NS**TV**NP**II**Y**A	398
H8	β_2AR	330	PD**FR**IAFQELL[C]	340
	CB_1	402	KDL**R**HAFRSMF[PSC]	412

The secondary structure was assigned by STRIDE (26). The C-terminal Cys residues of β_2AR and the CB_1 receptor, which are known to be palmitoylated in the lipid membrane environment, are represented in brackets. Conservancy of the aligned sequence by CLUSTALW (http://www.ebi.ac.uk/Tools/clustalw/) (65) is represented by consensus symbols: "*" for identical residues; ":" for conserved substitutions; and "." for semiconserved substitutions. Highly conserved residues in the rhodopsin family of GPCRs reported by Baldwin et al. (14) are in bold.

the TM helical domain (14). Structural information from the x-ray structures of rhodopsin (PDB code: 1U19) (18) and β_2AR (PDB code: 2RH1) (20) was also included. For construction of the helical bundle of the CB_1 receptor, the helical boundaries, not TM boundaries, of the x-ray structure of β_2AR (20) (Table 1) were used to extract the secondary structural information as much as possible. The helical boundaries were assigned by STRIDE (26). For loop I2 with the same residue length as β_2AR, the backbone coordinates were taken directly from the template x-ray β_2AR structure (20). For the loops similar in length (I1, E1, and E3) to the corresponding loops of β_2AR, a loop search method implemented in InsightII (Accelrys, San Diego, CA) was used to select a loop conformation resembling the corresponding loop in the β_2AR structure (20). For the long loops (E2 and I3), the comparative loop-building program Modeler (http://www.salilab.org/modeler/) (27) was used. These long loops deserve much attention in determining their conformations, but that was beyond the scope of this study. However, to obtain a more stable, realistic receptor model, all of the loops were included in this study because of the importance of the interconnecting loops in stabilizing the helix termini, as described in a recent study (28). For the N-terminal end, the first 10 residues from the N-terminus of H1 were retained to cover the extracellular side of the receptor, assuming that the N-terminal residues would not play a significant role in structure or function. For the C-terminal end, H8 right after H7 up to C^{415} was retained. Because it is known that this residue is palmitoylated in the lipid bilayer, the palmitoyl (PAL) moiety coordinated to C^{415} was included as part of the homology model of the CB_1 receptor to position near the intracellular membrane layer. All of the side chain conformations were determined by SCWRL (http://www1.jcsg.org/scripts/prod/scwrl/serve.cgi/) (29). An acetyl group and an N-methyl group were attached to the N-terminus and C-terminus, respectively, of the receptor model. The side chains of $E1.49^{133}$ and $D2.50^{163}$ were neutralized, whereas all other ionizable residues were in their ionization state at physiological conditions.

Simulation of the CB_1 receptor in a POPC lipid-bilayer

For construction of the CB_1 receptor within a lipid bilayer, the receptor was embedded in a 1-palmitoyl-2-oleoyl-*sn*-glycero-3-phosphocholine (POPC) bilayer guided by the innermost residues ($V1.47^{131}$, $A2.49^{162}$, $S3.39^{203}$, $M4.49^{240}$, $S5.48^{284}$, $I6.45^{353}$, and $T7.47^{391}$) of individual helices predicted by ZPRED (http://www.cbr.su.se/zpred/) (30). A typical size of the lipid was determined such that the receptor was surrounded by enough lipid molecules, typically with a space of ~20 Å between the protein and the cell boundary. The system was solvated using the SOLVATE plug-in in VMD (http://www.ks.uiuc.edu/Research/vmd/) (31) with a layer of 48 Å on both sides of the lipid bilayer. Then, sodium chloride molecules were used to ionize (0.5 M) and neutralize the system to satisfy electrostatic calculations. A total of ~68,000 atoms, including 14,625 water molecules, 140 lipids, 62 Na^+, and 77 Cl^-, resulted in a system of 80 Å × 98 Å × 98 Å for the protein-embedded POPC (Fig. 1 *A*).

Simulations were performed by the NAMD simulation package (version 2.6b2 for Linux-Power-MPI, http://www.ks.uiuc.edu/Research/namd/) (32), using CHARMM22 force-field parameters for the protein and the TIP3 water model (33,34), and CHARMM27 force-field parameters for the lipids (35). The required parameter set to describe the palmitoylated Cys was found in the literature (36). The temperature was maintained at 310 K by the use of Langevin dynamics (37) with a damping coefficient of 5/ps. The pressure was maintained at 1 atm by using the Nosé-Hoover method (38) with the modifications described in the NAMD User's Guide (http://www.ks.uiuc.edu/Research/namd/2.6/ug/). The van der Waals interactions were switched at 10 Å and zero smoothly at 12 Å. Electrostatic interactions were treated using the particle-mesh Ewald method (39). A pair list for calculating the van der Waals and electrostatic interactions was set to 13.5 Å and updated every 10 steps. A multiple timestepping integration scheme, the impulse-based Verlet-I (r-RESPA) method (40), was used to

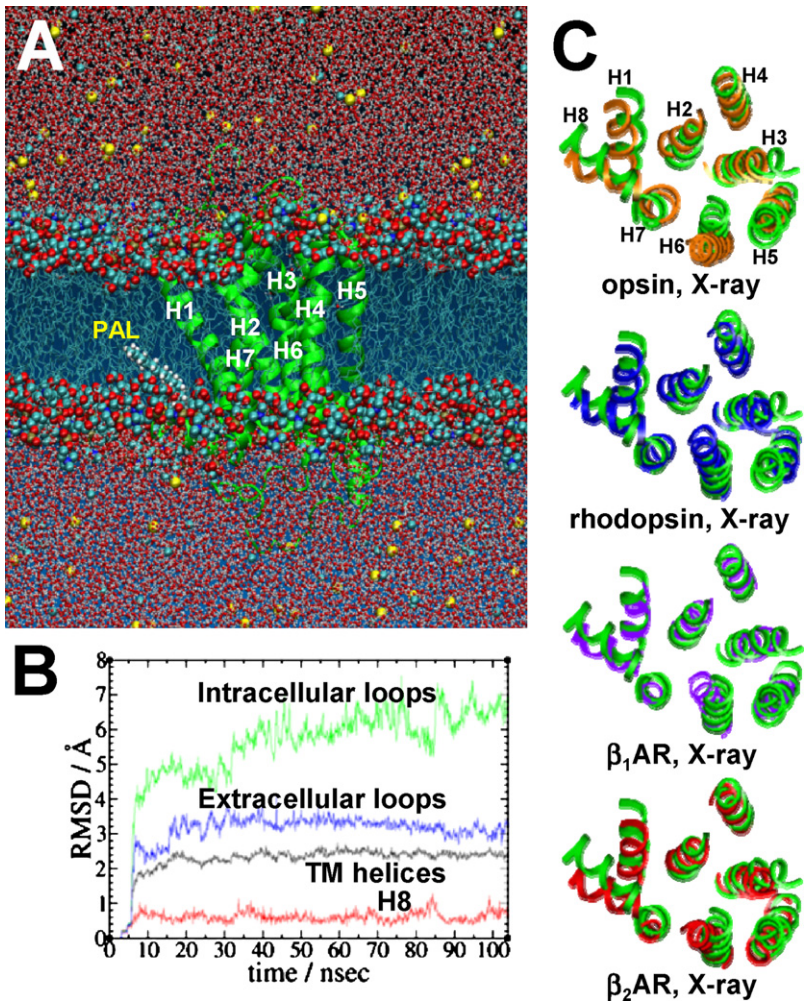

FIGURE 1 (*A*) Simulation system consisting of the CB_1 receptor, 140 POPC molecules, 14,625 water molecules, 62 Na^+, and 77 Cl^-. The PAL moiety that is covalently bonded to C^{415} is represented by space-filling. Lipid heads, water molecules, and ions are represented by space-filling, and lipid tails by sticks. Lipid hydrogen atoms are omitted for clarity. The system at 105 ns of the simulation is shown. Color coding: C, cyan; O, red; N, blue; P, orange; Na^+, cyan; Cl^-, yellow; and H, white. (*B*) The RMSDs, calculated by RMS fitting to the initial coordinates with respect to the backbone heavy atoms of the residues as defined in the helical boundaries, of the CB_1 receptor: TM helices (*black*), extracellular loops (*blue*), intracellular loops (*green*), and H8 (*red*). (*C*) Superposition of the CB_1 receptor (*green*) to the x-ray structures of opsin (17) (*orange*), rhodopsin (18) (*blue*), β_1AR (19) (*purple*), and β_2AR (20) (*red*), with respect to the Cα atoms of the TM helical domain.

efficiently compute full electrostatics. The timestep size for integration of each step of the simulation was 1 fs.

The system of the CB_1 receptor model embedded in a POPC bilayer was carefully equilibrated using a sequence of steps modified from the published procedure (41), as described below.

Step 1: After 2500 steps of minimization, the system was simulated at 310 K for 3 ns in the constant volume (NVT) ensemble, allowing only the lipid tails to be freed while other components were held fixed with a force constant of 2 kcal/mol$Å^2$ to obtain a fluid-like lipid bilayer (42).

Step 2: After 1000 steps of minimization, the system was simulated at 310 K for 1.5 ns in the constant pressure (NPT) ensemble with the protein constrained with a force constant of 2 kcal/mol$Å^2$ while other components were freed. For the first 0.5 ns of the simulation, an external force was applied such that water molecules were pushed out from the lipid hydrophobic region for better packing of the lipid tails. For the remaining 1.0 ns of the simulation, the external force applied for water was removed.

Step 3: After 1000 steps of minimization, the system was simulated at 310 K for 1.0 ns in the NPT ensemble with only the protein backbone constrained with a force constant of 2 kcal/mol$Å^2$. At the end of this stage, the lateral area became ~63 $Å^2$, which appeared to be in agreement with the experimentally measured values in the range of 63–68 $Å^2$ of the liquid-crystalline phase (43,44), which is the most biologically relevant phase (45).

Step 4: After 1000 steps of minimization, the system was simulated at 310 K for 100.0 ns in the NPT ensemble.

Step 5: The entire system was free to equilibrate and the lateral area of the box was kept fixed while the *z* dimension of the box was allowed to move freely. The structures taken every 100 ps of the simulation were used for the analysis.

RESULTS AND DISCUSSION

Convergence of the helical bundle of the CB_1 receptor

The CB_1 receptor in a POPC bilayer at the end of 105 ns simulation is shown in Fig. 1 *A*. To measure the structural stability of the CB_1 receptor model, the root mean-square deviations (RMSDs) were calculated over the performed simulation. As judged from the RMSDs shown in Fig. 1 *B* combined with the detailed structural analyses (see below), the helical bundle of the CB_1 receptor appears to be fully converged in 50 ns of the simulation. This study demonstrates the importance of performing longer simulations for enhanced conformational sampling (46) to ensure the receptor's full convergence. The finding that the RMSDs for the helical backbone are ~2.0 Å suggests that the helical bundle

TABLE 2 Frequently observed CB_1 receptor interactions contributing to the helical bundle stabilization at the late stage of the 105 ns MD simulation

Receptor interaction	Residues involved	van der Waals*	Electrostatic*	Nonbonding*	Interhelical stabilization
Interhelical H-bond†	$T1.46^{130}$/$T7.47^{391}$	−5.67(1.92)	−0.57(1.08)	−6.24(1.51)	H1/H7
	$E1.49^{133}$/$T7.47^{391}$	−6.14(2.44)	−0.34(1.02)	−6.48(2.02)	H1/H7
	$N1.50^{134}$/$S7.46^{390}$	−1.06(1.31)	−0.60(0.59)	−1.66(1.07)	H1/H7
	$S2.45^{158}$/$S3.42^{206}$	−6.72(1.66)	0.09(1.05)	−6.63(1.21)	H2/H3
	$D2.50^{163}$/$S3.39^{203}$	−2.12(2.10)	−0.43(0.36)	−2.55(2.12)	H2/H3
	$D2.50^{163}$/$N7.49^{393}$	−6.57(2.32)	0.02(1.08)	−6.55(1.79)	H2/H7
	$D2.50^{163}$/$S7.46^{390}$	−2.63(1.68)	−1.87(0.61)	−4.50(1.61)	H2/H7
	$S2.54^{167}$/$S7.46^{390}$	−2.58(1.70)	−0.22(0.86)	−2.80(1.32)	H2/H7
	$T1.46^{130}$/$S2.54^{167}$	−0.70(0.90)	−0.68(0.45)	−1.38(0.94)	H1/H2
	$N1.50^{134}$/$D2.50^{163}$	−1.68(1.03)	−1.29(0.31)	−2.97(0.99)	H1/H2
	$S2.45^{158}$/$W4.50^{241}$	−2.99(1.70)	−1.17(0.58)	−4.16(1.48)	H2/H4
	$Y3.51^{215}$/$Y5.56^{292}$	−2.76(2.76)	−1.29(0.80)	−4.04(2.50)	H3/H5
	$H3.55^{219}$/$Y5.60^{296}$	−0.49(2.17)	−1.37(0.55)	−1.86(2.02)	H3/H5
	$W6.48^{356}$/$C7.42^{386}$	−3.06(1.08)	−2.24(1.03)	−5.30(1.14)	H6/H7
	$W6.48^{356}$/$N7.45^{389}$	−2.14(1.65)	−1.93(0.95)	−4.07(1.64)	H6/H7
Water-mediated H-bond‡	$N1.50^{134}$/WAT1/ $D2.50^{163}$	0.57(1.17)	−6.29(2.84)	−5.72(2.27)	H1/H2
	WAT2/$T3.37^{201}$/ $T5.47^{283}$/WAT3	0.80(1.63)	−13.64(5.53)	−12.84(4.89)	H3/H5
	$Y5.39^{275}$/WAT4	−0.75(1.50)	−5.96(3.87)	−6.71(3.39)	—
	$T3.33^{197}$/WAT5	0.75(1.75)	−10.42(4.83)	−9.67(4.07)	—
	$C6.47^{355}$/WAT6/ $C7.38^{382}$/$C7.42^{386}$	0.79(1.46)	−9.73(2.39)	−8.94(1.99)	H6/H7
	WAT7/$Y7.53^{397}$/WAT8	−0.07(2.13)	−18.07(5.37)	−18.14(4.53)	—
Salt bridge†	$D2.63^{176}$/$K3.28^{192}$	−29.23(19.06)	0.07(1.07)	−29.16(18.32)	H2/H3
	$R3.50^{214}$/$D6.30^{338}$	−69.54(18.40)	1.24(1.99)	−68.30(17.17)	H3/H6
Aromatic stacking¶	$F3.44^{208}$/$F5.53^{289}$	−0.09(0.19)	−1.37(0.58)	−1.46(0.57)	H3/H5
	$Y3.51^{215}$/ $F5.53^{289}$	−0.08(0.25)	−1.49(0.44)	−1.57(0.55)	H3/H5
	$Y3.51^{215}$/$Y5.56^{292}$	−2.73(2.84)	−1.02(0.80)	−3.75(2.58)	H3/H5
	$Y3.51^{215}$/$Y5.60^{296}$	0.38(0.42)	−2.56(0.75)	−2.18(0.71)	H3/H5
	$F5.53^{289}$/$Y5.56^{292}$	−0.27(0.18)	−1.33(0.40)	−1.60(0.51)	—
	$Y5.56^{292}$/$Y5.60^{296}$	−0.44(0.41)	−1.25(0.48)	−1.69(0.74)	—
	$F2.57^{170}$/$F3.36^{200}$	−0.06(0.07)	−0.58(0.30)	−0.64(0.32)	H2/H3
	$F2.57^{170}$/$W6.48^{356}$	−0.04(0.14)	−1.50(0.45)	−1.54(0.48)	H2/H6
	$F3.36^{200}$/$W6.48^{356}$	−0.20(0.32)	−2.11(0.79)	−2.30(0.91)	H3/H6
Lipid insertion§	W^{279}/L^{287}/L^{288}/V^{291}/L^{352}/I^{353}/L^{360}	−0.84(1.12)	−10.60(1.59)	−11.45(2.10)	H5/H6
	L^{136}/V^{137}/V^{140}/L^{147}/P^{394}/I^{395}/A^{398}/A^{407}	−2.73(0.87)	−14.93(1.99)	−17.6(2.50)	H7/H8

*The energy values with the standard deviation of the values in parentheses were averaged over the last 50.0 ns of the simulation.
†Estimated by the nonbonding interaction energy between the residue pairs.
‡Estimated by the nonbonding interaction energy between the residue and the coordinated water molecule(s).
¶Estimated by the nonbonding interaction energy between the side chain aromatic rings.
§Estimated by the nonbonding interaction energy between the protein side chains and the lipid tails.

of the CB_1 receptor shows rather minor changes in structure. As shown in Fig. 1 *C*, superimposition of the helical bundle of the CB_1 receptor on the x-ray opsin (17), rhodopsin (18) β_1AR (19), and β_2AR (20) reveals that the helical bundle of the CB_1 receptor maintains a topology quite similar to that of other GPCRs overall.

H-bond networks

To examine the role of H-bonding interactions in the helical bundle of the CB_1 receptor, the numbers of the hetero atom contacts between the helical residues and the water molecules (a distance of <3.5 Å) were counted over the course of the simulation. The results revealed that the residues frequently involved in these interhelical H-bonds are $T1.46^{130}$/$T7.47^{391}$, $E1.49^{133}$/$T7.47^{391}$, and $N1.50^{134}$/$S7.46^{390}$ for H1/H7; $S2.45^{158}$/$S3.42^{206}$, and $D2.50^{163}$/$S3.39^{203}$ for H2/H3; $D2.50^{163}$/$N7.49^{393}$, $D2.50^{163}$/$S7.46^{390}$, and $S2.54^{167}$/$S7.46^{390}$ for H2/H7; $T1.46^{130}$/$S2.54^{167}$ and $N1.50^{134}$/$D2.50^{163}$ for H1/H2; $S2.45^{158}$/$W4.50^{241}$ for H2/H4; $Y3.51^{215}$/$Y5.56^{292}$ and $H3.55^{219}$/$Y5.60^{296}$ for H3/H5; and $W6.48^{356}$/$C7.42^{386}$ and $W6.48^{356}$/$N7.45^{389}$ for H6/H7. It is revealed that most of the residues involved in the interhelical H-bonds are known as the highly conserved residues of GPCRs (14). However, H2/H4, H3/H4, H3/H6, H3/H7, H4/H5, and H5/H6 show scarce or no H-bonding interactions. As shown in Table 2, the interhelical H-bonding energies between the H-bond pairs indicate that these interhelical H-bonds contribute significantly to interhelical stabilization.

Water molecules are often identified inside the helical core region near the polar or charged residues, or the surrounding backbone carbonyl O atoms that are unable to participate in the helical backbone H-bonding due to helical kinks. It appears that a water molecule on the extra- or intracellular

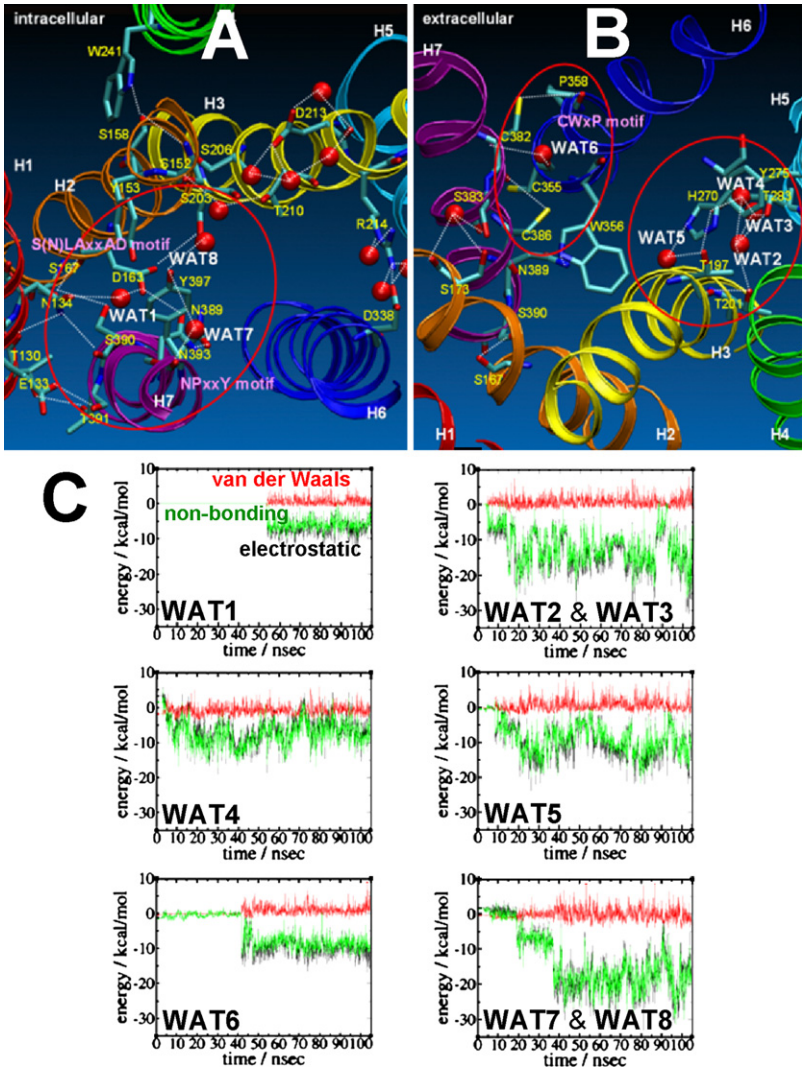

FIGURE 2 (*A*) H-bond networks, viewed from the intracellular side, of the helical bundle of the CB_1 receptor at the intracellular side. (*B*) H-bond networks, viewed from the extracellular side, of the helical bundle of the CB_1 receptor at the extracellular side. The H-bonds are represented by broken lines (*white*), whereas the water-mediated, clustered H-bond networks are circled by continuous lines (*red*). All water molecules (*red*) are represented in the space-filling mode. Hydrogen atoms are omitted for clarity. The structure was taken at 105 ns of the simulation. (*C*) Energy stabilization by water-mediated H-bond networks is estimated by nonbonding interaction energy (in kcal/mol) (in *green*), which is a summation of the electrostatic (*black*) and van der Waals (*red*) components. As the H-bonding partner, see Table 2. Color coding for the TM helices (*ribbons*): red, H1; orange, H2; yellow, H3; green, H4; cyan, H5; blue, H6; purple, H7; and gray, H8.

surface of the receptor is initially attracted through the long-range electrostatic interactions, presumably by the charged/polar residues within the receptor helical bundle, and enter into the receptor core region along the path transiently formed by the electrochemical gradient during the dynamic equilibrium process of the intermolecular interactions between the protein and waters. Indeed, the present MD simulation of the fully hydrated POPC bilayer with the embedded CB_1 receptor shows that a few water molecules form a stable coordination to specific residues within the helical bundle (see below), whereas most of the water molecules remain as bulk solvents. In this study, several well-developed H-bond networks and their closely associated water molecules, defined as WAT1–WAT8, were identified inside the helical core, as described below.

Near the S(N)LAxAD motif

In the middle of the interhelical region of H1/H2/H7, a large, complex H-bond network is formed: $N1.50^{134}$/$D2.50^{163}$ via WAT1 for an indirect, water-mediated H-bonding pair, and $T1.46^{130}$/$N1.50^{134}$, $T1.46^{130}$/$T7.47^{391}$, $E1.49^{133}$/$T7.45^{391}$, $N1.50^{134}$/$S7.46^{390}$, $D2.50^{163}$/$S2.54^{167}$, $D2.50^{163}$/$S3.39^{203}$, $D2.50^{163}$/$S7.46^{390}$, $D2.50^{163}$/$N7.49^{393}$, $S2.54^{167}$/$S7.46^{390}$, and $N7.45^{389}$/$N7.49^{393}$ for direct H-bonding pairs (Fig. 2 *A*). It is very surprising to note that this H-bond network includes many highly conserved residues at H1, H2, and H7 of GPCRs (14). This H-bond network resembles the reported H-bond network of rhodopsin, connecting $N1.50^{55}$, $D2.50^{83}$, and $N7.49^{302}$, that has been proposed to modulate ligand binding to G-protein coupling (47). Existing deep inside the helical core, WAT1 appears to be similar to wat1b, which has been identified as one of the coordinated water molecules in the rhodopsin x-ray structure (48). Energy stabilization by WAT1 in forming two H-bonds to $N1.50^{134}$ and $D2.50^{163}$ is estimated to be −5.72 kcal/mol (Fig. 2 *C* and Table 2). Extended from this H-bond network, $S2.45^{158}$ of the S(N)LAxAD motif forms H-bonds with $S3.42^{206}$ and $W4.50^{241}$ (see Table 2) and stabilizes the interhelical interaction between H2 and H3/H4 close to the membrane-water interfacial region (Fig. 2 *A*).

Near the extracellular side of H3/H5

It is shown that at least four water molecules (WAT2–WAT5) that mediate a large H-bond network exist in the extracellular core region of H3/H5 (Fig. 2 *B*). WAT2 and WAT3 form four H-bonds to T3.37^{201} and T5.47^{283}. Energy stabilization by WAT2 and WAT3 in forming these H-bonds is estimated to be −12.84 kcal/mol (Fig. 2 *C* and Table 2). Similarly, energy stabilization by WAT4 in forming two H-bonds to Y5.39^{275} is estimated to be −6.71 kcal/mol (Fig. 2 *C* and Table 2). Extended from this water-mediated network, T3.33^{197} forms a direct H-bond to Y5.39^{275} and an indirect H-bond to H5.34^{270} mediated by a water molecule. WAT5, located rather close to the extracellular surface, forms H-bonds with T3.33^{197} and H5.34^{270}. The energy stabilization by WAT5 in forming two H-bonds to T3.33^{197} is estimated to be −9.67 kcal/mol (Fig. 2 *C* and Table 2).

Near the CWxP motif

Of interest, a water molecule (WAT6) is identified that is trapped in a space surrounded by C6.47^{355}, C7.38^{382}, and C7.42^{386} (Fig. 2 *B*). WAT6 appears to be quite similar to the x-ray wat3 that forms H-bonds to C6.47^{264}, Y6.51^{268}, and P7.38^{291} of rhodopsin (48). Apparently, WAT6 is coordinated to the backbone oxygen of C6.47^{355}, which is not able to form the backbone H-bond due to P6.58^{358}. It is revealed that C7.38^{382} forms a direct H-bond to C7.42^{386} and an indirect H-bond to C6.47^{355} mediated by WAT6. The energy stabilization by WAT6 in forming two H-bonds to C7.38^{382} and C7.42^{386} is estimated to be −8.93 kcal/mol (Fig. 2 *C* and Table 2). In considering the importance of the highly conserved CWxP motif, as the rotameric toggle switch (49), WAT6 appears to have a role in modulating the receptor during the G-protein activation process. It is revealed that a water molecule, not far away from the CWxP motif, is frequently coordinated to S2.60^{173}, which forms H-bonds with D^{266} and S7.39^{383} (Fig. 2 *B*). A recent mutation study suggested that S7.39^{383} was important for the binding of classical cannabinoids (50). According to the CB_1 receptor model presented here, the breakage of the H-bonding of S7.39^{383} to S2.60^{173} would affect the H2/H7 helical interaction such that the proposed ligand-binding pocket (51) at the extracellular side might be disrupted.

Near the NPxxY motif

The above-mentioned H-bond network near the S(N)LAxxAD motif includes several H7 residues, most of which are in close proximity to the NPxxY motif, one of the most highly conserved motifs of many GPCRs (52). WAT7 and WAT8 are directly coordinated to Y7.53^{397} of the NPxxY motif. The energy stabilization by WAT7 and WAT8 in forming four H-bonds to Y7.53^{397} is estimated to be −18.14 kcal/mol (Fig. 2 *C* and Table 2). Because the backbone oxygen atom of T7.47^{391} cannot form the backbone H-bond due to P7.50^{394}, it instead forms an H-bond to the side chain carboxylate hydrogen atom of E1.49^{133}, which leads H1 and H7 in this region to be quite closely packed (Fig. 2 *A*).

Conserved water contact sites

Located close to the highly conserved residues (14), the identified coordinated water molecules, whose contact sites are often conserved (53), appear to have structural and functional significance (50,54). The results presented here indicate that unless a water molecule has the perfect orientation to satisfy all the required H-bonds in forming coordination inside the helical bundle, it will not be retained within the bilayer. For example, a water molecule initially approaches D2.50^{163} in 20.0 ns of the simulation and occupies a space between D2.50^{163} and N7.49^{393} transiently due to a misfit. In 50.0 ns of the simulation, WAT1 approaches a space between N1.50^{134} and D2.50^{163}, forms a very stable coordination to them, and stays for the rest of the simulation (Fig. 3 *A*), as indicated by two H-bonds to N1.50^{134} and D2.50^{163} (Fig. 3 *B*). Such stable coordination of WAT1 would be important for maintaining the H-bond network in H1/H2/H7, centered at highly conserved D2.50^{163} of the S(N)LAxAD motif and N7.49^{393} of the NPxxY motif.

Similarly, a water molecule occupies a space between L7.43^{387} and N7.45^{389} around the CWxP motif transiently during 5–25 ns of the simulation, and then another water molecule (WAT6) enters in 40 ns of the simulation, mediating H-bonds to C6.47^{355}, C7.38^{382}, and C7.42^{386}. WAT6 at the CWxP motif appears to assist in stabilizing H6/H7 such that C7.38^{382} and C7.42^{386} maintain H-bonds to W6.48^{356}, securing the side chain tryptophan ring of W6.48^{356} in a specific orientation (i.e., the χ_1 angle ~ −60°) as the inactive form of the receptor (49).

Other protein interactions

Salt bridges

It has been proposed that the salt bridge between R3.50^{135} and E6.30^{247} of rhodopsin, as the ionic lock, maintains the inactive state of the rhodopsin class of GPCRs mainly through H6 stabilization (55). Such a salt bridge is identified in the rhodopsin x-ray structure (18), but not in either the opsin (17) or β_2AR (20) x-ray structure. It is quite interesting to see that the present CB_1 receptor model using the x-ray structure of β_2AR forms the salt bridge between R3.50^{214} and E6.30^{338}. It should be noted that the finding that D2.63^{176} forms salt bridges with K3.28^{192} is in agreement with a recent mutation study suggesting that D2.63^{176} of the CB_1 receptor contributes to the receptor structure and function through the charge interaction (56). These salt bridges contribute significantly to interhelical stabilization as estimated by the nonbonding interaction energies of −68.30 kcal/mol for R3.50^{214}/E6.30^{338} and −29.16 kcal/mol for D2.63^{176}/K3.28^{192} (Table 2).

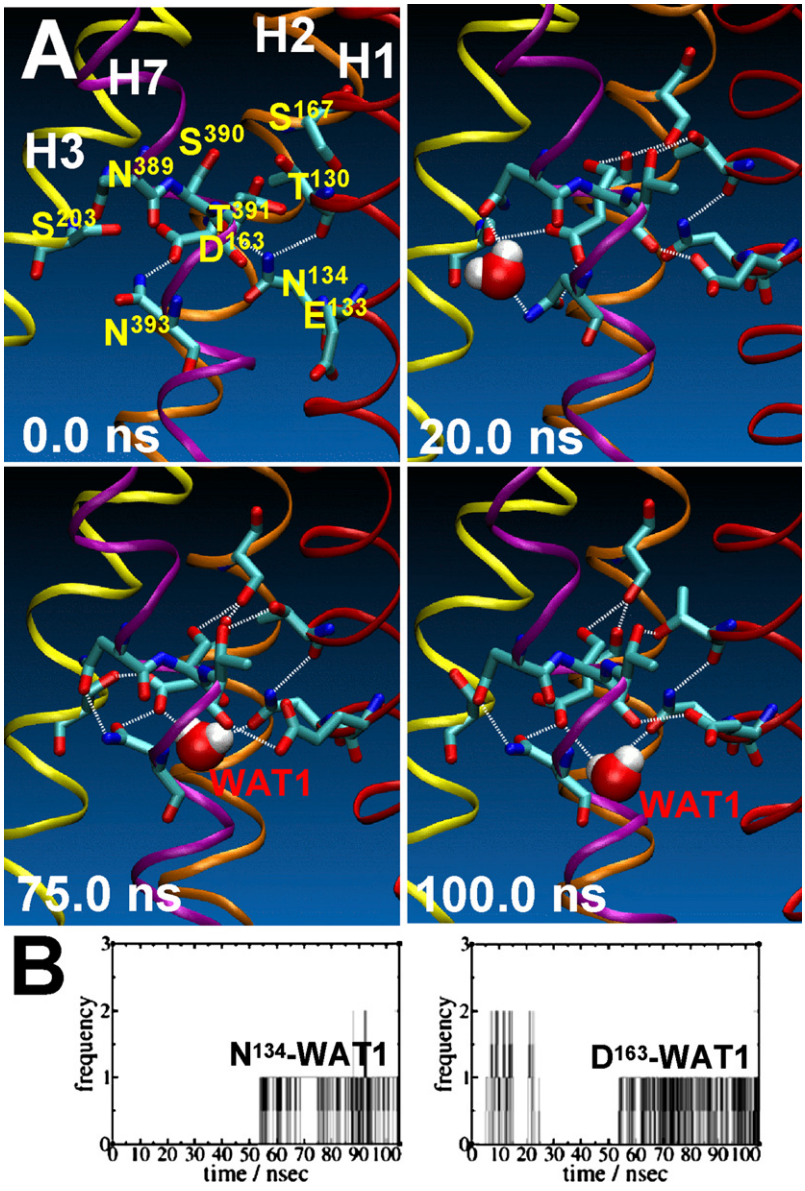

FIGURE 3 (*A*) Snapshots of the conserved water contact site in the middle of the helical core of H1/H2/H7 near the S(N)LAxAD motif at 0.0 ns, 20.0 ns, 75.0 ns, and 100.0 ns of the simulation are represented. (*B*) WAT1 coordination to both N1.50^{134} and D2.50^{163} during the simulation.

Aromatic stacking

Aromatic interactions are known to be one of the major forces that stabilize protein complex association (57) and are considered to enhance helix-helix association for IMPs (58). It is shown from the present CB_1 receptor model that some aromatic residues inside the helical core form both intra- and interhelical aromatic clusters, For example, the cluster formed by the aromatic residues around Y3.51^{215}, including F3.44^{208}, F5.53^{289}, Y5.56^{292}, and Y5.60^{296}, appears to be important for stabilizing H3/H5 association at the intracellular region, as indicated by the fact that stacking of these aromatic residues is achieved as the simulation proceeds (Fig. 4 *A*). With the energy contribution of −12.25 kcal/mol by six stacking interactions (Table 2), the individual aromatic-aromatic residue pairs are ~1.5~2.0 kcal/mol, which is in agreement with reported interaction energy values for the benzene dimer (59). Compared with the other aromatic-aromatic residue pairs showing that the major source of aromatic stacking is van der Waals forces, the Y3.51^{215}/Y5.56^{292} pair provides a much higher energy contribution due to an increased contribution of the electrostatic component by the ring hydroxyls (Fig. 4 *B*).

Another example of the aromatic stacking interaction is illustrated by an aromatic cluster around W6.48^{356}, including F2.57^{170} and F3.36^{200}, of the CWxP motif that has been proposed as the toggle switch (49) crucial for G-protein activation. It is revealed that the energy contribution of the F3.36^{200}/W6.48^{356} pair is higher compared to the other pairs, which is in agreement with a recent study suggesting the importance of the F3.36^{200}/W6.48^{356} interaction in receptor activation (60).

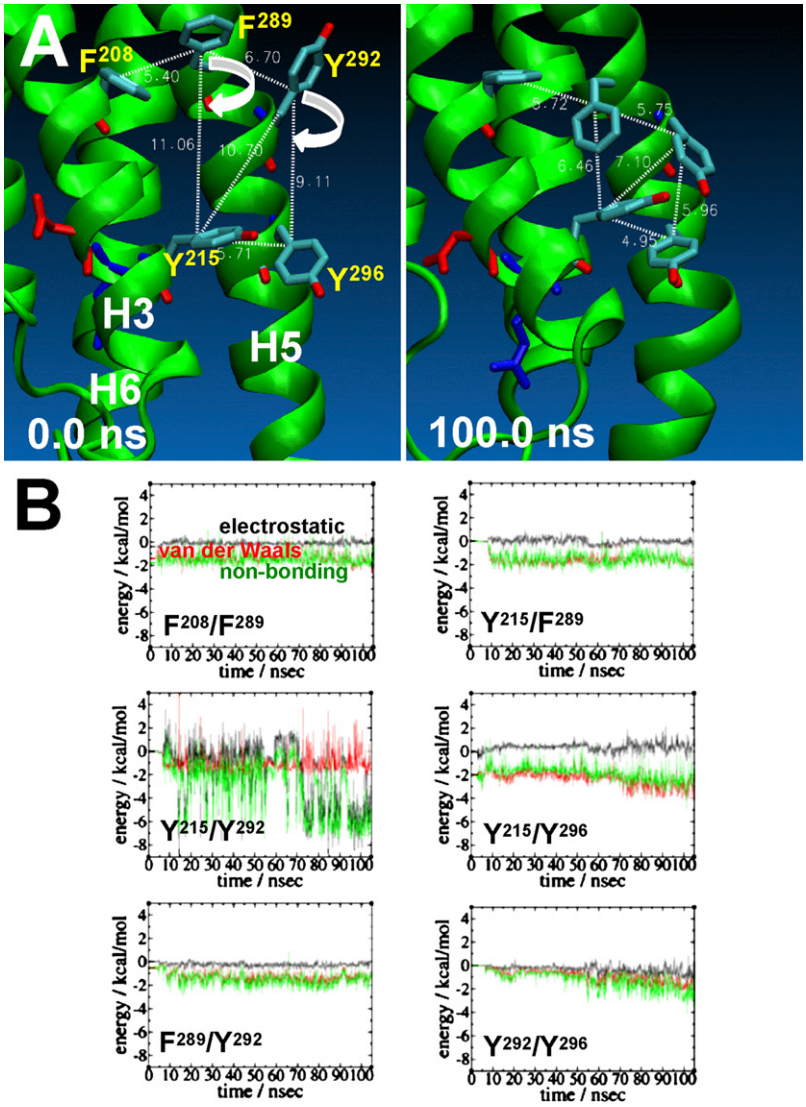

FIGURE 4 (*A*) Development of the aromatic cluster near the D(E)RY motif by F3.44^{208}, Y3.51^{215}, F5.53^{289}, Y5.56^{292}, and Y5.60^{296} is shown by a comparison of the snapshots taken at the time of 0.0 ns and 100.0 ns of the simulation. D3.49^{213} (*red*) and R3.50^{214} (*blue*) are also represented. (*B*) Energy stabilization by the aromatic stacking interactions between the individual aromatic stacking pairs. Only the side chain was considered for nonbonding interaction energy.

Protein-lipid interactions inside the helical core region

Lipid interaction with the hydrophobic pocket-forming residues in the middle of H5 and H6

This study shows that H5 and H6 in the middle of the helical bundle are rather loosely packed due to the kink of H6 induced by P6.50^{358} of the CWxP motif, and form a pocket by hydrophobic residues, including W5.43^{279}, L5.51^{287}, L5.52^{288}, V5.55^{291}, L6.44^{352}, I6.45^{353}, and L6.52^{360}, together with F3.36^{200} and V3.40^{204} (Fig. 5 *A*). It is revealed that this hydrophobic pocket is quickly (in 20 ns) occupied by a lipid tail that remains in the pocket for the rest of the simulation, with its tail penetrating into the pocket as deep as ~10 Å from the receptor/lipid interface. As a result, the lipid can reach the ligand-binding pocket in the core region (Fig. 5 *A*), implying its potential role in ligand binding and receptor function. The stabilization of H5/H6 by this lipid tail is rather significant (>-10 kcal/mol) (Table 2) when compared with the earlier structures with an unoccupied or partially occupied hydrophobic pocket (see Fig. 5 *B*). This example demonstrates that lipids play an important role in stabilizing IMPs by directly interacting with the protein residues.

It has been proposed that the molecular constraints imposed on the inactive state of the receptor by some of the functional motifs need to be released for receptor activation (61). In the same context, a rotamer toggle switch by C6.47/W6.48/F6.52 of β_2AR (49) or by W6.48/F3.36 of the CB_1 receptor (60) that modulates the pro-kink of H6 in association with the receptor activity has been proposed. Based on the present CB_1 receptor model, the rotameric angles of W6.48^{356} appears to be extremely well conserved throughout the simulation: the χ_1 angle maintains about $-60°$ (i.e., g^+), in agreement with the χ_1 angle of W6.48 of the x-ray structures of rhodopsin (18) and β_2AR (20). It

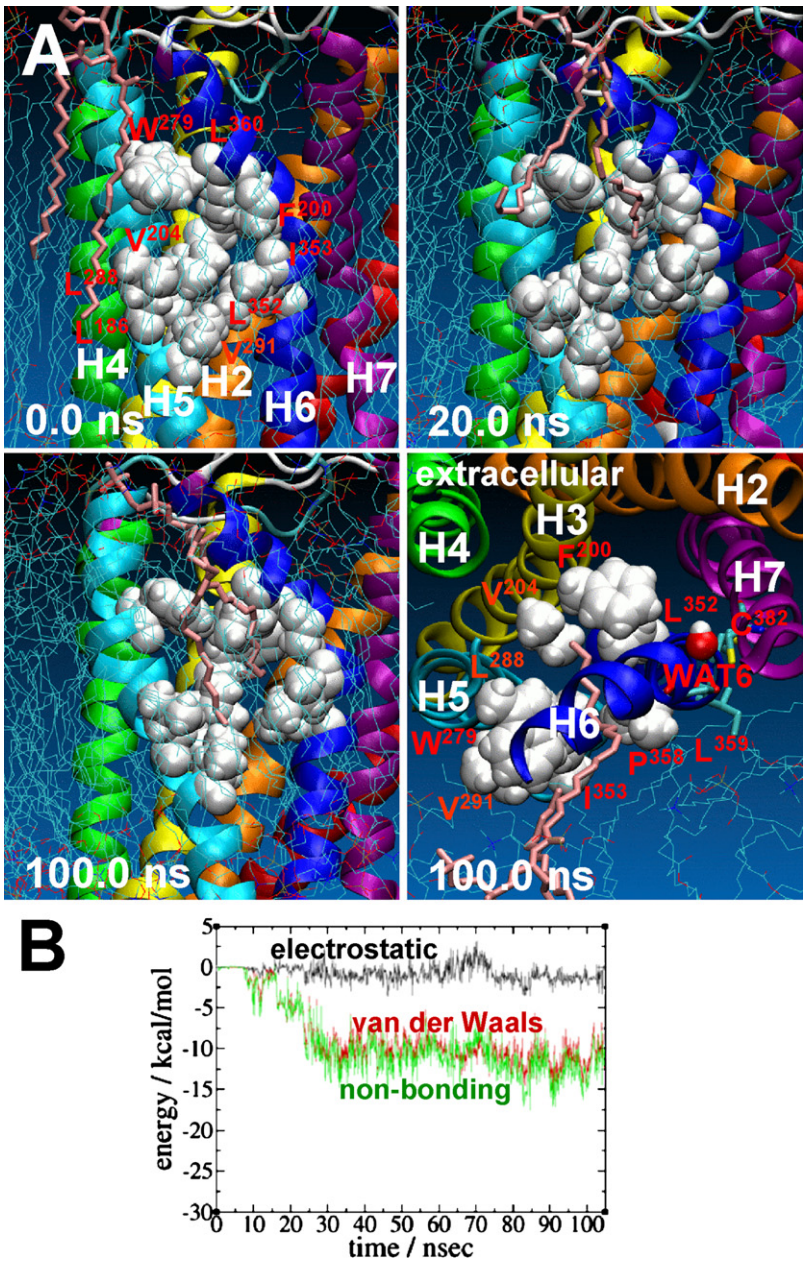

FIGURE 5 (*A*) The hydrophobic pore-forming residues, including F3.36^{200}, V3.40^{204}, W5.43^{279}, L5.52^{288}, V5.55^{291}, L6.44^{352}, I6.45^{353}, and L6.52^{360}, at the H5/H6 kinked region in the middle of the helical bundle are represented by white space-filling. The kink-causing P6.50^{358} and part of the residues (L6.51^{359}and C7.38^{382}) that form H-bonds to WAT6 are represented by sticks. The coordinated water WAT6 is represented by space-filling. The lipid, whose tails are inserted into the hydrophobic pore, is represented by pink sticks. The nonbonding interactions between these hydrophobic pore-forming residues and the lipid tails are traced along the simulation at: 0.0 ns, 20.0 ns, 100.0 ns (*side view*), and 100.0 ns (*extracellular view*). For the snapshot of 100.0 ns (*extracellular view*), the intracellular half of the lipid bilayer and L6.52^{360} are omitted for clarity. Color coding for the TM helices (*ribbons*) is the same as in Fig. 2 *A*. (*B*) Nonbonding interaction energy (in kcal/mol) between the hydrophobic pore-forming residues, including F3.36^{200}, V3.40^{204}, W5.43^{279}, L5.52^{288}, V5.55^{291}, L6.44^{352}, I6.45^{353}, and L6.52^{360}, and a lipid that is found to be in close contact. Color coding for the TM helices (*ribbons*) is the same as in Fig. 2 *A*.

appears that W6.48^{356} of the CB_1 receptor is stabilized not only by the neighboring aromatic residues, such as F2.57^{170} and F3.36^{200}, but also by an H-bond to N7.45^{389} (see Table 2). Thus, it is likely that ligand binding would disrupt the aromatic stacking of W6.48^{356} with F2.57^{170} and F3.36^{200}, and at the same time the H-bond of W6.48^{356} with N7.45^{389}, causing the tryptophan ring moiety of W6.48^{356} to become flipped around. Ultimately, H6 would be able to move around to make the necessary rigid-body rotation required for G-protein activation (62).

It has been proposed that V6.43^{351}/I6.46^{354} as a βXXβ motif forms a hydrophobic groove as an initial interaction site of the CB_1 receptor for the endogenous cannabinoid ligand N-arachidonylethanolamine (AEA) (63). The MD simulation and the lipid-protein contact analysis reveal that the V6.43^{351}/I6.46^{354} pair, together with L6.39^{347} of H6 and L7.44^{388}, V7.48^{392}, and I7.52^{396} of H7, where the kink induced by P7.50^{394} exists, forms a recessed edge for good hydrophobic interactions with lipid tails. It appears that the V6.43^{351}/I6.46^{354} pair alone would not be sufficient to form a groove and function as the interaction site for AEA.

Lipid interaction with the hydrophobic pore-forming residues at the H7/H8 junction

The NPxxY(x)$_{5,6}$F motif of rhodopsin has been proposed as one of key structural motifs in providing constraints to stabilize the H7/H8 junction area through the aromatic stacking interaction between Y7.53^{306} and F7.60^{313} (52). Although

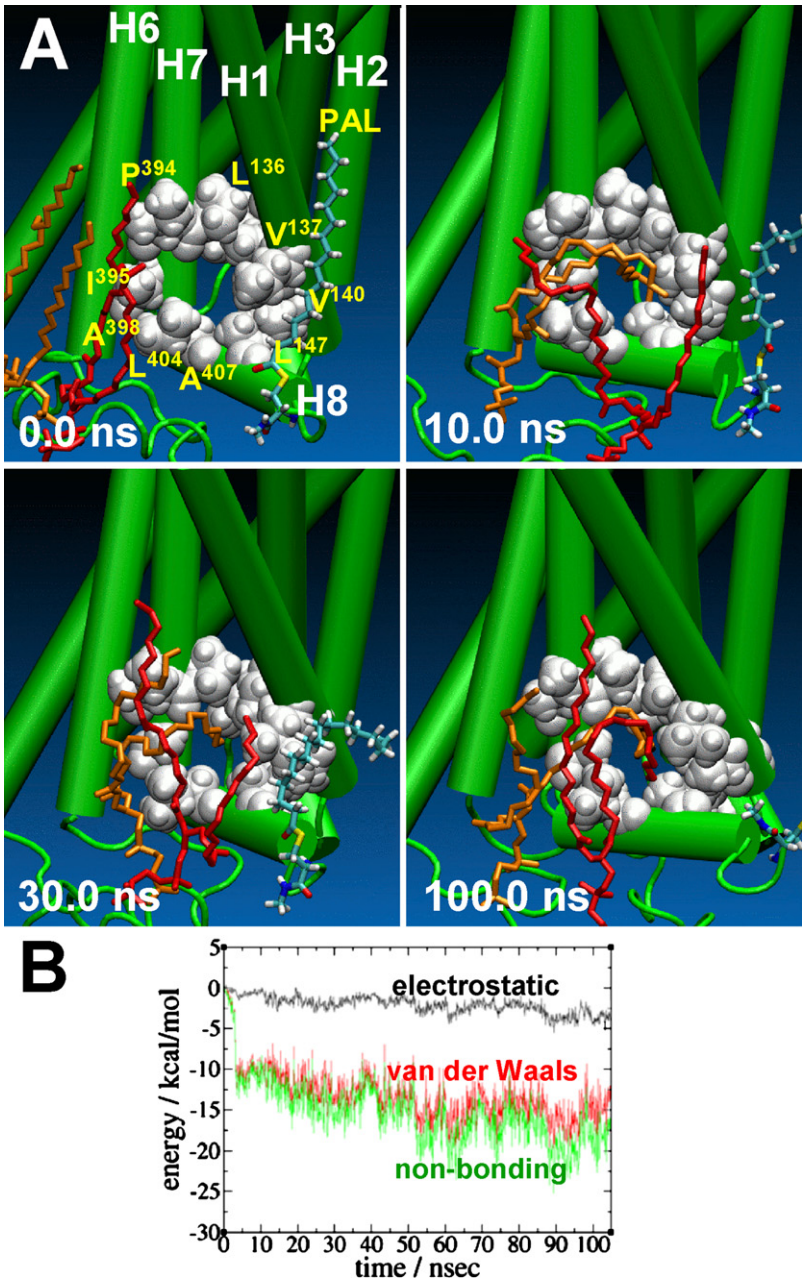

FIGURE 6 (*A*) The hydrophobic pore-forming residues, including L1.52^{136}, V1.53^{137}, V1.56^{140}, L^{147}, P7.50^{394}, I7.51^{395}, A7.54^{398}, L^{404}, and A^{407}, at the H7/H8 junction are represented by white space-filling. The two lipids, whose tails are inserted into the hydrophobic pore, are represented by orange and red sticks. The helical bundle is represented by the green cartoon. The PAL moiety that is covalently bonded to C^{415} is represented by sticks. The nonbonding interactions between these hydrophobic pore-forming residues and the lipid tails are traced along the simulation at 0.0 ns, 10.0 ns, 30.0 ns, and 100.0 ns. Color coding for the palmitoylated C^{415}: C, cyan; O, red; N, blue; P, orange; and S, yellow. (*B*) Nonbonding interaction energy (in kcal/mol) between the hydrophobic pore-forming residues, including L1.52^{136}, V1.53^{137}, V1.56^{140}, L^{147}, P7.50^{394}, I7.51^{395}, A7.54^{398}, L^{404}, and A^{407}, and the two lipids in close contact.

such aromatic interaction is impossible in the CB_1 receptor due to the 7.60 position being replaced by a Leu residue (i.e., L^{404}), a recent mutation study of L^{404} of the CB_1 receptor demonstrated that this residue is necessary for maximum activity of the receptor (64). Thus, it appears that L^{404} has a unique pattern of interaction other than aromatic stacking. Our analysis of the CB_1 receptor model reveals that L^{404} interaction with A7.54^{398} is well maintained throughout the simulation and its interaction with the lipids increases significantly over the course of the simulation. A closer examination reveals that L^{404}, together with neighboring hydrophobic residues, including L1.52^{136}, V1.53^{137}, V1.56^{140}, L^{147}, P7.50^{394}, I7.51^{395}, A7.54^{398}, and A^{407}, forms a hydrophobic pocket at the H7/H8 junction (Fig. 6 *A*). It appears that this pocket is so hydrophobic that it attracts hydrophobic tails of the surrounding lipids at the early stage of the simulation and retains strong hydrophobic interactions throughout the simulation (Fig. 6 *A*). It is revealed that the stabilization by the lipid-protein hydrophobic pocket interaction is −17.6 kcal/mol (Table 2). Thus, it appears that the lipid interactions with the hydrophobic residues at the H7/H8 junction play an important role in stabilizing H8 at the membrane-water interface.

CONCLUSIONS

This study on the helical bundle of the CB_1 receptor reveals that the receptor residues, most of which are highly

conserved and form functional motifs in many GPCRs (14), are involved in several of the distinct types of molecular interactions that maintain the inactive state of the CB_1 receptor. Within the bilayer exist several extensive, water-mediated H-bond networks, where the coordinated water molecules play crucial roles in minimizing the exposure of the polar or charged residues, which is unfavorable in the extreme hydrophobic environment within the bilayer (2). Several well-developed aromatic stacking interactions that are important for stabilizing the helix-helix association are identified. It is also found that several lipid tails interact tightly with the hydrophobic residues in the gap of H5/H6 and at the H7/H8 junction. It is likely that the flexible, dynamic nature of these lipid-protein interactions would be advantageous for a prompt adjustment of the associated helices when their rigid-body motions are required for transferring the molecular signal to the coupled G-proteins. In summary, the results presented here suggest that all of these specific interactions among the protein, water, and lipids that stabilize the helical structure can be considered as the molecular constraints that maintain the inactive state of the CB_1 receptor. Disruption of these specific interactions would be necessary to release the molecular constraints to achieve a conformational change of the receptor suitable for G-protein activation.

I thank Drs. L. Padgett and A. Howlett for their careful reading of the manuscript, and Drs. T. Darden, E. Tajkhorshid, B. Thomas, Z. Ohkubo, and L. Perera for many helpful discussions. I also appreciate the technical assistance of Mr. J. Rudd in analyzing and processing the simulation data.

This work was performed with the use of the Big Red IBM e1350 cluster (Indiana University) and partially supported by the National Institute on Drug Abuse (K01-DA020663) and the National Science Foundation through TeraGrid Resources by Indiana University (MCB080037N).

REFERENCES

1. Popot, J. L., and D. M. Engelman. 2000. Helical membrane protein folding, stability, and evolution. *Annu. Rev. Biochem.* 69:881–922.
2. Engelman, D. M., Y. Chen, C. N. Chin, A. R. Curran, A. M. Dixon, et al. 2003. Membrane protein folding: beyond the two stage model. *FEBS Lett.* 555:122–125.
3. Lüneberg, J., M. Widmann, M. Dathe, and T. Marti. 1998. Secondary structure of bacteriorhodopsin fragments. External sequence constraints specify the conformation of transmembrane helices. *J. Biol. Chem.* 273:28822–28830.
4. Yeagle, P. L., G. Choi, and A. D. Albert. 2001. Studies on the structure of the G-protein-coupled receptor rhodopsin including the putative G-protein binding site in unactivated and activated forms. *Biochemistry.* 40:11932–11937.
5. Schneider, D. 2004. Rendezvous in a membrane: close packing, hydrogen bonding, and the formation of transmembrane helix oligomers. *FEBS Lett.* 577:5–8.
6. Hunt, J. F., T. N. Earnest, O. Bousché, K. Kalghatgi, K. Reilly, et al. 1997. A biophysical study of integral membrane protein folding. *Biochemistry.* 36:15156–15176.
7. Lazarova, T., K. A. Brewin, K. Stoeber, and C. R. Robinson. 2004. Characterization of peptides corresponding to the seven transmembrane domains of human adenosine A_2a receptor. *Biochemistry.* 43: 12945–12954.
8. Marti, T. 1998. Refolding of bacteriorhodopsin from expressed polypeptide fragments. *J. Biol. Chem.* 273:9312–9322.
9. Pitman, M. C., A. Grossfield, F. Suits, and S. E. Feller. 2005. Role of cholesterol and polyunsaturated chains in lipid-protein interactions: molecular dynamics simulation of rhodopsin in a realistic membrane environment. *J. Am. Chem. Soc.* 127:4576–4577.
10. Nyholm, T. K., S. Ozdirekcan, and J. A. Killian. 2007. How protein transmembrane segments sense the lipid environment. *Biochemistry.* 46:1457–1465.
11. Gether, U. 2000. Uncovering molecular mechanisms involved in activation of G protein-coupled receptors. *Endocr. Rev.* 21:90–113.
12. Drews, J. 2002. Drug discovery: a historical prospective. *Science.* 287:1960–1964.
13. Probst, W. C., L. A. Snyder, D. I. Schuster, J. Brosius, and S. C. Sealfon. 1992. Sequence alignment of the G-protein coupled receptor superfamily. *DNA Cell Biol.* 11:1–20.
14. Baldwin, J. M., G. F. Schertler, and V. M. Unger. 1997. An α-carbon template for the transmembrane helices in the rhodopsin family of G-protein-coupled receptors. *J. Mol. Biol.* 272:144–164.
15. Ballesteros, J. A., and H. Weinstein. 1995. Integrated methods for modeling G-protein coupled receptors. *In* Methods in Neuroscience. P. M. Conn and S. C. Sealfon, editors. Academic Press, San Francisco, CA, 366–428.
16. Kratochwil, N. A., P. Malherbe, L. Lindemann, M. Ebeling, M. C. Hoener, et al. 2005. An automated system for the analysis of G protein-coupled receptor transmembrane binding pockets: alignment, receptor-based pharmacophores, and their application. *J. Chem. Inf. Model.* 45:1324–1336.
17. Park, J. H., P. Scheerer, K. P. Hofmann, H. W. Choe, and O. P. Ernst. 2008. Crystal structure of the ligand-free G-protein-coupled receptor opsin. *Nature.* 454:183–187.
18. Okada, T., M. Sugihara, A. N. Bondar, M. Elstner, P. Entel, et al. 2004. The retinal conformation and its environment in rhodopsin in light of a new 2.2 Å crystal structure. *J. Mol. Biol.* 342:571–583.
19. Warne, T., M. J. Serrano-Vega, J. G. Baker, R. Moukhametzianov, P. C. Edwards, et al. 2008. Structure of a β1-adrenergic G-protein-coupled receptor. *Nature.* 454:486–491.
20. Cherezov, V., D. M. Rosenbaum, M. A. Hanson, S. G. Rasmussen, F. S. Thian, et al. 2007. High-resolution crystal structure of an engineered human β2-adrenergic G protein-coupled receptor. *Science.* 318:1258–1265.
21. Devane, W. A., F. A. Dysarz III, M. R. Johnson, L. S. Melvin, and A. C. Howlett. 1988. Determination and characterization of a cannabinoid receptor in rat brain. *Mol. Pharmacol.* 34:605–613.
22. Matsuda, L. A., S. J. Lolait, M. J. Brownstein, A. C. Young, and T. I. Bonner. 1990. Structure of a cannabinoid receptor and functional expression of the cloned cDNA. *Nature.* 346:561–564.
23. Howlett, A. C. 2005. Cannabinoid receptor signaling. *Handb. Exp. Pharmacol.* 168:53–79.
24. Notredame, C., D. G. Higgins, and J. Heringa. 2000. T-Coffee: a novel method for fast and accurate multiple sequence alignment. *J. Mol. Biol.* 302:205–217.
25. Joost, P., and A. Methner. 2002. Phylogenetic analysis of 277 human G-protein-coupled receptors as a tool for the prediction of orphan receptor ligands. *Genome Biol.* 3:1–16.
26. Frishman, D., and P. Argos. 1995. Knowledge-based protein secondary structure assignment. *Proteins.* 23:566–579.
27. Fiser, A., R. K. G. Do, and A. Sali. 2000. Modeling of loops in protein structures. *Protein Sci.* 9:1753–1773.
28. Ulmschneider, M. B., D. P. Tieleman, and M. S. Sansom. 2005. The role of extra-membranous inter-helical loops in helix-helix interactions. *Protein Eng. Des. Sel.* 18:563–570.
29. Canutescu, A. A., A. A. Shelenkov, and R. L. Dunbrack, Jr. 2003. A graph-theory algorithm for rapid protein side-chain prediction. *Protein Sci.* 12:2001–2014.

30. Granseth, E., H. Viklund, and A. Elofsson. 2006. ZPRED: predicting the distance to the membrane center for residues in α-helical membrane proteins. *Bioinformatics*. 22:e191–e196.

31. Humphrey, W., A. Dalke, and K. Schulten. 1996. VMD—visual molecular dynamics. *J. Mol. Graph.* 14:33–38.

32. Phillips, J. C., R. Braun, W. Wang, J. Gumbart, E. Tajkhorshid, et al. 2005. Scalable molecular dynamics with NAMD. *J. Comput. Chem.* 26:1781–1802.

33. Brooks, B. R., R. E. Bruccoleri, B. D. Olafson, D. J. States, S. Swaminathan, et al. 1983. CHARMM: a program for macromolecular energy minimization, and dynamics calculations. *J. Comput. Chem.* 4:187–217.

34. MacKerell, A. D.Jr., D. Bashford, M. Bellott, R. L. Dunbrack Jr., J. Evanseck, et al. 1998. All-atom empirical potential for molecular modeling and dynamics studies of proteins. *J. Phys. Chem. B.* 102:3586–3616.

35. Feller, S., and A. D. MacKerell, Jr. 2000. An improved empirical potential energy function for molecular simulations of phospholipids. *J. Phys. Chem. B.* 104:7510–7515.

36. Saam, J., E. Tajkhorshid, S. Hayashi, and K. Schulten. 2002. Molecular dynamics investigation of primary photoinduced events in the activation of rhodopsin. *Biophys. J.* 83:3097–3112.

37. Feller, S. E., Y. Zhang, R. W. Pastor, and B. R. Brooks. 1995. Constant pressure molecular dynamics simulation: the Langevin piston method. *J. Chem. Phys.* 103:4613–4621.

38. Hoover, W. G. 1985. Canonical dynamics: Equilibrium phase-space distributions. *Phys. Rev. A.* 31:1695–1697.

39. Essmann, U., L. Perera, M. L. Berkowitz, T. Darden, H. Lee, et al. 1995. A smooth particle-mesh Ewald method. *J. Chem. Phys.* 103:8577–8593.

40. Tuckerman, M., and B. J. Berne. 1992. Reversible multiple time scale molecular dynamics. *J. Chem. Phys.* 97:1990–2001.

41. Gumbart, J., and K. Schulten. 2006. Molecular dynamics studies of the archaeal translocon. *Biophys. J.* 90:2356–2367.

42. Heller, H., M. Schaefer, and K. Schulten. 1993. Molecular dynamics simulation of a bilayer of 200 lipids in the gel and in the liquid crystal phase. *J. Phys. Chem.* 97:8343–8360.

43. König, B., U. Dietrich, and G. Klose. 1997. Hydration and structural properties of mixed lipid/surfactant model membranes. *Langmuir.* 13:525–532.

44. Kucerka, N., Y. Liu, N. Chu, H. I. Petrache, S. Tristram-Nagle, et al. 2005. Structure of fully hydrated fluid phase DMPC and DLPC lipid bilayers using X-ray scattering from oriented multilamellar arrays and from unilamellar vesicles. *Biophys. J.* 88:2626–2637.

45. White, S. H., and M. C. Wiener. 1996. The liquid crystallographic structure of fluid lipid bilayer membranes. *In* Membrane Structure and Dynamics. K. M. Merz and B. Roux, editors. Birkhäuser, Boston, MA. 127–144.

46. Grossfield, A., S. E. Feller, and M. C. Pitman. 2007. Convergence of molecular dynamics simulations of membrane proteins. *Proteins.* 67:31–40.

47. Lehmann, N., U. Alexiev, and K. Fahmy. 2007. Linkage between the intramembrane H-bond network around aspartic acid 83 and the cytosolic environment of helix 8 in photoactivated rhodopsin. *J. Mol. Biol.* 366:1129–1141.

48. Okada, T., Y. Fujiyoshi, M. Silow, J. Navarro, E. M. Landau, et al. 2002. Functional role of internal water molecules in rhodopsin revealed by X-ray crystallography. *Proc. Natl. Acad. Sci. USA.* 99:5982–5987.

49. Shi, L., G. Liapakis, R. Xu, F. Guarnieri, J. A. Ballesteros, et al. 2002. β2 adrenergic receptor activation. Modulation of the proline kink in transmembrane 6 by a rotamer toggle switch. *J. Biol. Chem.* 277:40989–40996.

50. Kapur, A., D. P. Hurst, D. Fleischer, R. Whitnell, G. A. Thakur, et al. 2007. Mutation studies of Ser7.39 and Ser2.60 in the human CB1 cannabinoid receptor: evidence for a serine-induced bend in CB1 transmembrane helix 7. *Mol. Pharmacol.* 71:1512–1524.

51. Picone, R. P., A. D. Khanolkar, W. Xu, L. A. Ayotte, G. A. Thakur, et al. 2005. (-)-7′-Isothiocyanato-11-hydroxy-1′,1′-dimethylheptylhexahydrocannabinol (AM841), a high-affinity electrophilic ligand, interacts covalently with a cysteine in helix six and activates the CB1 cannabinoid receptor. *Mol. Pharmacol.* 68:1623–1635.

52. Fritze, O., S. Filipek, V. Kuksa, K. Palczewski, K. P. Hofmann, et al. 2003. Role of the conserved $NPxxY(x)_{5,6}F$ motif in the rhodopsin ground state and during activation. *Proc. Natl. Acad. Sci. USA.* 100:2290–2295.

53. Renthal, R. 2008. Buried water molecules in helical transmembrane proteins. *Protein Sci.* 17:293–298.

54. Pardo, L., X. Deupi, N. Dölker, M. L. López-Rodríguez, and M. Campillo. 2007. The role of internal water molecules in the structure and function of the rhodopsin family of G protein-coupled receptors. *ChemBioChem.* 8:19–24.

55. Ballesteros, J. A., A. D. Jensen, G. Liapakis, S. G. Rasmussen, L. Shi, et al. 2001. Activation of the β2-adrenergic receptor involves disruption of an ionic lock between the cytoplasmic ends of transmembrane segments 3 and 6. *J. Biol. Chem.* 276:29171–29177.

56. Kapur, A., P. Samaniego, G. A. Thakur, A. Makriyannis, and M. E. Abood. 2008. Mapping the structural requirements in the CB1 cannabinoid receptor transmembrane helix II for signal transduction. *J. Pharmacol. Exp. Ther.* 325:341–348.

57. Meyer, E. A., R. K. Castellano, and F. Diederich. 2003. Interactions with aromatic rings in chemical and biological recognition. *Angew. Chem. Int. Ed. Engl.* 42:1210–1250.

58. Johnson, R. M., K. Hecht, and C. M. Deber. 2007. Aromatic and cation-π interactions enhance helix-helix association in a membrane environment. *Biochemistry.* 46:9208–9214.

59. Tsuzuki, S., K. Honda, T. Uchimaru, M. Mikami, and K. Tanabe. 2002. Origin of attraction and directionality of the π/π interaction: model chemistry calculations of benzene dimer interaction. *J. Am. Chem. Soc.* 124:104–112.

60. McAllister, S. D., D. P. Hurst, J. Barnett-Norris, D. Lynch, P. H. Reggio, et al. 2004. Structural mimicry in class A G protein-coupled receptor rotamer toggle switches: the importance of the F3.36(201)/W6.48(357) interaction in cannabinoid CB1 receptor activation. *J. Biol. Chem.* 279:48024–48037.

61. Palczewski, K. 2006. G protein-coupled receptor rhodopsin. *Annu. Rev. Biochem.* 75:743–767.

62. Farrens, D. L., C. Altenbac, K. Yang, W. L. Hubbell, and H. G. Khorana. 1996. Requirement of rigid-body motion of transmembrane helices for light activation of rhodopsin. *Science.* 274:768–770.

63. Lynch, D. L., and P. H. Reggio. 2006. Cannabinoid CB1 receptor recognition of endocannabinoids via the lipid bilayer: molecular dynamics simulations of CB1 transmembrane helix 6 and anandamide in a phospholipid bilayer. *J. Comput. Aided Mol. Des.* 20:495–509.

64. Anavi-Goffer, S., D. Fleischer, D. P. Hurst, D. L. Lynch, J. Barnett-Norris, et al. 2007. Helix 8 Leu in the CB1 cannabinoid receptor contributes to selective signal transduction mechanisms. *J. Biol. Chem.* 282: 25100–25113.

65. Larkin, M. A., G. Blackshields, N. P. Brown, R. Chenna, P. A. McGettigan, et al. 2007. ClustalW and ClustalX version 2. *Bioinformatics.* 23:2947–2948.